

¹ e-mail: christoph.naegerl@uibk.ac.at

Key words Bose-Einstein condensation

arXiv:cond-mat/0408268v1 [cond-mat.other] 12 Aug 2004²

Optimized production of a cesium Bose-Einstein condensate

Tobias Kraemer¹, Jens Herbig¹, Michael Mark¹, Tino Weber¹, Cheng Chin¹, Hanns-Christoph Nägerl^{1*}, and Rudolf Grimm^{1,2}

¹Institut für Experimentalphysik, Universität Innsbruck, Technikerstraße 25, A-6020 Innsbruck, Austria

²Institut für Quantenoptik und Quanteninformation, Österreichische Akademie der Wissenschaften, A-6020 Innsbruck, Austria

Received: date / Revised version: date

Abstract We report on the optimized production of a Bose-Einstein condensate of cesium atoms using an optical trapping approach. Based on an improved trap loading and evaporation scheme we obtain more than 10^5 atoms in the condensed phase. To test the tunability of the interaction in the condensate we study the expansion of the condensate as a function of scattering length. We further excite strong oscillations of the trapped condensate by rapidly varying the interaction strength.

PACS: 03.75.Kk; 32.80.Pj

1 Introduction

Much of the present work in the field of quantum gases relies on optical trapping techniques and on the ability to tune atomic interactions. Optical approaches have been recently employed in several atomic Bose-Einstein condensation experiments [1, 2, 3, 4, 5] and in experiments on the production of ultracold molecular samples [6, 7, 8, 9, 10] and on molecular Bose-Einstein condensates [11, 12]. The major advantages in optical traps are the possibility to trap atoms in any sublevel of the electronic ground state and the ease to adjust the interaction strength using magnetically induced Feshbach resonances.

The cesium atom is very attractive for experiments with tunable atomic interactions. The lowest internal quantum state of Cs features a unique combination of wide and narrow Feshbach resonances which are easily accessible at low magnetic fields [13]. This results in a great flexibility for tuning the atomic scattering properties. In particular, magnetic tuning of the interaction strength has recently allowed the first realization of a Bose-Einstein condensate (BEC) with Cs atoms [4] and the realization of a two-dimensional condensate very close to a dielectric surface [5]. The tunability of the atomic interaction can be exploited in experiments where one might wish to adjust or to dynamically change the mean-field interaction of the condensate. Also, the Feshbach resonances can be used to produce molecules from an atomic BEC [14, 8,

9, 10] and to study the transition from an atomic BEC to a molecular BEC. In this context, a quantum phase transition with an essentially topological character has been predicted [15, 16]. For such and many other intriguing experiments it is desirable to have a large BEC of Cs atoms as a starting point.

In this paper we report on the optimized production of an essentially pure Cs BEC in the lowest internal quantum state with more than 10^5 atoms. Since this state cannot be trapped by purely magnetic means, the path to condensation relies on a sequence of optical traps. We discuss the loading and transfer from one trap to the next and give a detailed description of the evaporation path and of the resulting condensate. As a demonstration for tunability we measure the expansion energy as a function of scattering length in time-of-flight experiments. In particular, we show the ultra-slow expansion of the condensate after release from the trap for nearly vanishing scattering length. The release energy corresponds to ~ 50 pK. Finally, we present first results when the scattering length is suddenly stepped and the condensate then starts to oscillate freely in the trap.

2 Cesium scattering properties and Feshbach resonances

Early experiments [17, 18] towards condensation of cesium focused on samples in magnetic traps polarized either in the upper hyperfine ground state $F = 4$, magnetic sublevel $m_F = 4$, or in the lower hyperfine state $F = 3$, $m_F = -3$. Here, F denotes the total angular momentum and m_F the magnetic quantum number. The spin relaxation rates were measured to be several orders of magnitude higher than expected [19, 20, 21]. It was later understood that this is caused by the dipolar relaxation process induced by the second-order spin-orbit interaction [22]. The maximum phase-space density in a small sample of Cs atoms was a factor of about four away from condensation [23].

The problem of the strong inelastic two-body losses can be overcome by using the lowest internal state of cesium,

* corresponding author

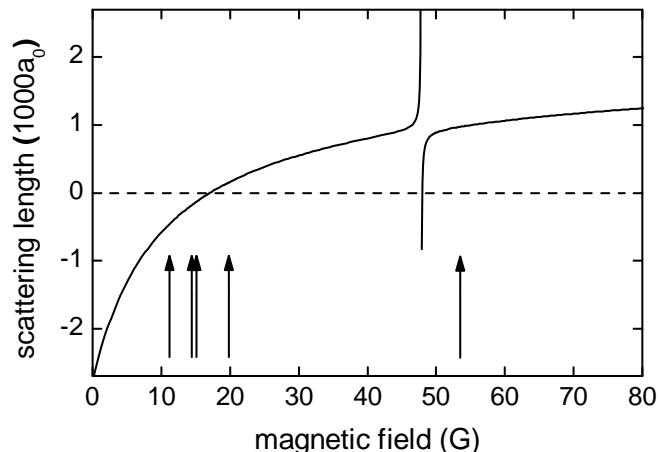


Fig. 1 Scattering length as a function of magnetic field for the state $F = 3, m_F = 3$. There is a relatively broad Feshbach resonance at 48.0 G due to coupling to a d-wave molecular state. The arrows indicate several very narrow resonances at 11.0, 14.4, 15.0, 19.9 and 53.5 G, which result from coupling to g-wave molecular states. The data is taken from [13].

energy according to energy and momentum conservation. The atoms that form the molecule are usually lost, and the third atom is either lost or it deposits its share of the binding energy in the sample. Heating of the sample is the combination of “anti-evaporation” and recombination heating [28]. To a good approximation, the three-body recombination rate scales with the fourth power of the scattering length. Unfortunately, the prefactor in this scaling law is measured to be relatively large [28]. To minimize this heating, the recombination products should be removed quickly from the trap. It is thus important to assure that the sample is not operated too deep in the hydrodynamic regime and that the evaporation is efficient in *all* directions. Arbitrarily increasing the scattering length to speed up the forced evaporation is therefore not possible without sacrificing cooling efficiency. Within these limits, tuning the scattering length allows for an optimization of the evaporation for given trap parameters. For example, for the low initial densities in a large reservoir trap the evaporation may be sped up by increasing the scattering length. In a later trapping stage with a higher atomic density the scattering length should be reduced to optimize the ratio of good to bad collisions.

3 BEC production

3.1 Overview of experimental strategy

For producing large condensates in optical dipole traps, it is necessary to independently optimize both trap loading and evaporative cooling. For initial loading of as many atoms as possible, an optical trap with large volume is needed which, in view of limited laser power, implies a shallow trapping potential. For subsequent forced evaporative cooling, however, high densities and fast elastic collisions require much tighter confinement. These two requirements in general demand dynamical changes of the trapping potential. A possible way to implement this is a spatial compression of the optical trap using e.g. a zoom-lens system [29]. Our approach is based on an alternative way where a sequence of optical trapping schemes is used to provide optimized loading together with optimized evaporative cooling.

We first use a shallow, large volume CO₂-laser trap as a “reservoir” for collecting the atoms before forced evaporative cooling is implemented in a tighter trap. The reservoir trap can be efficiently loaded with atoms that are precooled by Raman-sideband cooling [30]. This approach allows collection of atoms at moderate densities with little loss from three-body collisions and with negligible heating from either photon scattering or trap vibrations. It serves as a good starting point for the final transfer into a tighter optical trap. The tighter trap is adiabatically increased and adds a “dimple” to the trapping potential of the reservoir. Collisional loading of this dimple already yields a significant enhancement of the local number and phase-space density [31]. After turn-

1 $F = 3, m_F = 3$ [24,25,26,27]. In this state, all inelastic
 2 two-body processes are endothermic and are thus fully
 3 suppressed at sufficiently low temperature. This state
 4 requires optical trapping since it cannot be captured
 5 in a magnetic trap. Optically trapped atoms can only
 6 be efficiently evaporated by lowering the total poten-
 7 tial depth. This process weakens the confinement of the
 8 trapped sample and thus makes it difficult to achieve
 9 sufficiently high elastic collision rates for effective evap-
 10 oration. Hence, adjustability of the collisional properties
 11 is very helpful for a fast evaporation strategy.

12 The success in condensing Cs [4] largely relies on the fact
 13 that the s-wave scattering length for the $F = 3, m_F = 3$
 14 state can be tuned to moderate and positive values by
 15 the application of relatively low dc magnetic fields [13].
 16 As Fig. 1 shows, an external magnetic field allows for
 17 precise tuning of the atomic scattering length a from
 18 negative to positive values. Positive scattering lengths in
 19 the range between zero and one thousand a_0 are attained
 20 for magnetic fields of a few ten Gauss; a_0 denotes Bohr’s
 21 radius. In particular, there is a gentle zero-crossing of the
 22 scattering length near 17 G [25]. Here, the interaction
 23 of atoms in a BEC is effectively switched off. Several
 24 narrow higher-order Feshbach resonances [13], caused by
 25 coupling to d- and g-wave molecular states, enable very
 26 rapid control of the atomic scattering properties. With
 27 the magnetic field being a free parameter in our optical
 28 trapping approach, we can take full advantage of this
 29 tunability of the s-wave scattering length.

30 For Cs in the $F = 3, m_F = 3$ ground state the process
 31 of three-body recombination is the dominant loss and
 32 heating mechanism [28]. In a recombination process,
 33 three atoms collide, two of them form a molecule, and
 34 the third atom takes away two thirds of the binding en-

ing off the reservoir trap excellent conditions for further
forced evaporative cooling are obtained.

The different trap stages of optical trapping used in our
experiments are illustrated in Fig. 2. An overview of the
evolution of phase-space density and particle number for
the various trapping stages is shown in Fig. 3.

The use of relatively weak optical trapping necessitates
the implementation of magnetic “levitation” where a
magnetic field gradient along the vertical direction com-
pensates for the gravitational force. This levitation turns
out to be very useful in two ways: First, in the limit of
very weak optical trapping only one spin state is held
in the trap. This assures perfect spin polarization of the
sample¹. Further, efficient evaporation can be performed
without the effect of gravitational sag in the trap. The dc
magnetic field offset remains a free parameter for flexible
tuning of the scattering length.

3.2 Laser cooling

The initial collection and cooling of Cs atoms is achieved
by conventional techniques. In a stainless steel vacuum
chamber [32] atoms are loaded into a magneto-optical
trap (MOT) from a Zeeman slowed atomic beam with
up to 3×10^8 atoms after about 6 s. The MOT is oper-
ated on the $6^2S_{1/2}, F = 4$ to $6^2P_{3/2}, F' = 5$ transi-
tion. The ultra-high vacuum of less than 1×10^{-11} mbar
gives 200 s for the $1/e$ -lifetime of the MOT. The MOT
light is derived from a high power laser diode² referenced
via beat-lock to a grating-stabilized master diode laser.
Standard absorption imaging is used to determine par-
ticle numbers and temperatures.

We compress the atomic cloud by ramping up the mag-
netic field gradient in the MOT by a factor of 5 to 33
G/cm within 40 ms. Simultaneously we linearly change
the detuning of the MOT laser from around 10 MHz
to 30 MHz. At the end of the ramp, we switch off the
MOT light and the magnetic field gradient. To cool the
compressed cloud, we then apply degenerate Raman-
sideband cooling [30] in an optical lattice to further cool
and to polarize the atoms in the desired $F = 3, m_F = 3$
state. We have adapted the technique as described in [33]
to our setup. This cooling scheme is particularly suited
for polarizing atoms in the $F = 3, m_F = 3$ state be-
cause this is a dark state for which photon scattering is
suppressed. Four laser beams derived from an injection
locked slave laser resonant with the $F = 4$ to $F' = 4$
transition produce a three-dimensional optical lattice,
drive Raman-sideband transitions and repump out of
the $F = 4$ ground state manifold. The total power of
all the four beams is 65 mW and their $1/e^2$ -beam radii
are about 1 mm. The oscillation frequency in the lat-
tice is on the order of 100 kHz. A small magnetic field
offset of several hundred mG is applied to induce the
Raman-sideband cooling. We succeed in polarizing 90%
of the atoms. The ensemble is then adiabatically released
from the lattice after 6 ms of cooling time. If the atomic
cloud is released into free space, the temperature of the

ensemble with up to 4×10^7 atoms is about $0.7 \mu\text{K}$. For
our typical atomic densities this corresponds to a phase
space density of 1×10^{-3} .

3.3 Reservoir trap

We generate the large reservoir trap by horizontally cross-
ing two CO₂-laser beams A₁ and A₂ at right angles as
shown in Fig. 2(a). At the same time we apply a mag-
netic gradient field in the vertical direction to levitate
the atoms against gravity. The delivered powers in laser
beams A₁ and A₂ are 90 W and 65 W, respectively.
The light comes from two separate, highly stable lin-
early polarized single-frequency CO₂-lasers³. Switching
of the beams is done by external acousto-optical mod-
ulators⁴ (AOMs). A₁ is downshifted in frequency by 40
MHz, whereas A₂ is upshifted by 40 MHz to prevent any
interference. To avoid mode-hops the cooling water for
the lasers needs to be stabilized to better than ± 20 mK.
Still, a slow mode drift changes the power of the lasers
by a few percent over the time scale of minutes. At the
crossing point the $1/e^2$ -beam radii of the two lasers are
(605 ± 35) μm and (690 ± 35) μm .

The magnetic fields for levitation and for Feshbach tun-
ing are generated by two pairs of coils (aligned with their
axes parallel to the vertical direction. One pair in anti-
Helmholtz configuration produces the vertical magnetic
field gradient near 31.3 G/cm to levitate the atoms in the
 $F = 3, m_F = 3$ state. Another pair in Helmholtz config-
uration provides a variable bias field B_0 of up to 200 G.
The combined field results in a weak outward directed
force $F(\rho) = m\alpha^2\rho$ depending on the horizontal distance
 ρ from the vertical symmetry axis. For perfect levitation
of our atoms the constant $\alpha = g\sqrt{m/(3\mu_B B_0)}$ describes
the curvature of the parabolic anti-trapping potential.
The levitation field thus slightly reduces the trap depth
along the horizontal direction. Here, m is the mass of
Cs, g is the gravitational acceleration, and μ_B is Bohr’s
magneton. At $B_0 = 17$ G we have $\alpha = 2\pi \times 3.4$ Hz. The
horizontal trap frequencies $\omega_{x,y}$ are reduced according
to $\omega'_{x,y} = \sqrt{\omega_{x,y}^2 - \alpha^2}$. This is usually a very small effect
for all but the lowest trap frequencies. Note that levi-
tation also affects the horizontal motion of free atoms
after the optical trap is shut off. The horizontal motion
follows $\rho(t) = \rho_0 \cosh(\alpha t) + \alpha^{-1}v_0 \sinh(\alpha t)$ for initial
position ρ_0 and initial velocity v_0 . The vertical motion
is not affected.

We excite vertical trap oscillations by briefly changing
the vertical magnetic field gradient and hence tilting the
trap. For exciting horizontal trap oscillations we shift the
equilibrium position of the atoms by adding a horizon-
tal magnetic field component. In both cases we monitor
the center-of-mass oscillation of the atomic cloud after
50 ms time-of-flight. The geometrically averaged trap
frequency $\bar{\nu}$ is calculated to be (12.6 ± 1.5) Hz which
is in good agreement with the experimental value of
(13.2 ± 0.2) Hz. Together with the levitation and the
magnetic bias field the lasers provide an effective trap

¹ This Stern-Gerlach separation technique also allows for
radio-frequency evaporation along the vertical direction. Al-

³ Coherent-DEOS GEM-100L

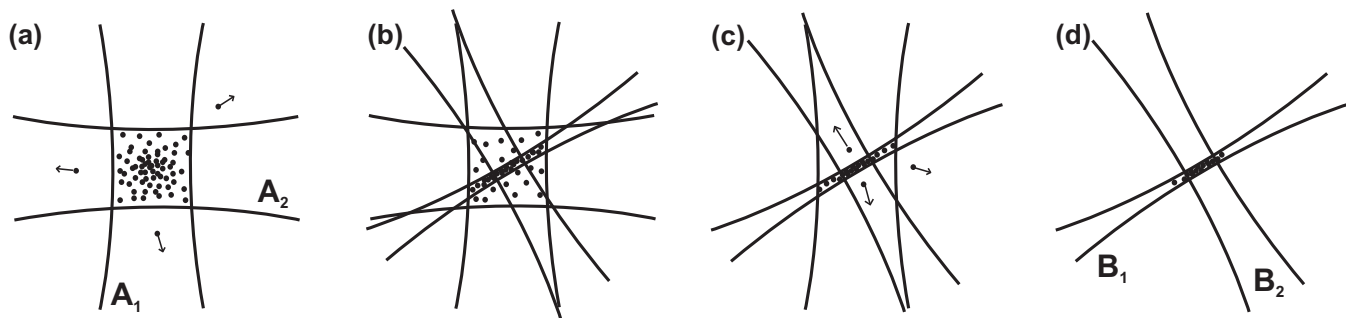


Fig. 2 Illustration of the various stages of trap loading and evaporative cooling as seen from above. (a) Plain evaporation in a crossed CO₂-laser trap generated by beams A₁ and A₂ at a scattering length of $a = 1215 a_0$. (b) 1.5 s of ramping and collisional loading into a crossed 1064-nm fibre laser trap generated by beams B₁ and B₂ with a final scattering length $a = 210 a_0$. (c) Forced evaporative cooling after switching off CO₂-laser beam A₂. The power of all remaining lasers is ramped down, and the power in CO₂-laser beam A₁ is reduced to zero. (d) Final configuration of the crossed 1064-nm trap. Imaging is done in the horizontal plane at an angle of 30° with respect to the long axis of the cigar-shaped atomic cloud.

1 depth of about $k_B \times 7 \mu\text{K}$. This trap depth is given by 39
 2 the weaker of the two CO₂-lasers as the atoms can escape 40
 3 along the direction of the stronger beam. 41

4 For transfer of the precooled atoms into the reservoir 42
 5 trap, we leave the light of the two CO₂-lasers on dur- 43
 6 ing the entire pre-cooling phase. This is because the 44
 7 CO₂-lasers show strong variations in beam pointing and 45
 8 beam shape as a function of radio-frequency power to 46
 9 the AOMs. We have checked that the small light shift 47
 10 introduced by the lasers does not affect the initial load- 48
 11 ing and cooling efficiency. The reservoir trap is then acti- 49
 12 vated by ramping up the magnetic field and its gradient. 50
 13 The $1/e$ -rise time of the magnetic fields is limited to 1.5 51
 14 ms because of eddy currents in the stainless steel cham- 52
 15 ber. We therefore do not expect the transfer to be fully 53
 16 adiabatic. 54

17 We find that the atoms are heated to about $2.2 \mu\text{K}$ by 55
 18 the transfer into the reservoir trap. A clear measurement 56
 19 on the trapped sample is only possible after about 50 ms 57
 20 since the system initially is not in thermal equilibrium 58
 21 and since the untrapped atoms need to disappear from 59
 22 the field of view. We largely attribute the heating to im- 60
 23 perfect phase space matching. In fact, the atomic cloud 61
 24 after Raman-sideband cooling to $0.7 \mu\text{K}$ has a $1/e$ -radius 62
 25 of $\sim 350 \mu\text{m}$. In comparison, an equilibrium distribution 63
 26 in the reservoir trap at $0.7 \mu\text{K}$ would have a $1/e$ -radius 64
 27 of $\sim 100 \mu\text{m}$. Potential energy is thus gained which is 65
 28 then turned into kinetic energy, effectively heating the 66
 29 cloud of atoms. Subsequently, the hot atoms evaporate 67
 30 out of the trap. For this phase of plain evaporation we 68
 31 set the magnetic bias field to 73.5 G. The scattering len- 69
 32 gth is then $1215 a_0$. The temperature is reduced to less 70
 33 than $1 \mu\text{K}$ within 10 s. After this time, we measure more 71
 34 than 4×10^6 atoms, corresponding to a peak phase space 72
 35 density of 2×10^{-3} . 73

3.4 Dimple trap

37 We proceed with loading of the dimple trap after 2 s of 75
 38 plain evaporation in the reservoir trap. At this point the 76

atom number is 7.8×10^6 and the phase space density is 89
 1.7×10^{-3} (see Fig. 3). The dimple trap is generated by 90
 horizontally intersecting one tightly focused laser beam 91
 B₁ with $34\text{-}\mu\text{m}$ waist and another less focused beam B₂ 92
 with $260\text{-}\mu\text{m}$ waist at right angles, rotated by 30° in the 93
 horizontal plane with respect to the CO₂-laser beams 94
 as shown in Fig. 2(d). This is different from our ear- 95
 100 lier work [4] where we have used CO₂-laser beam A₂ for 96
 axial confinement. We introduce the B₂ beam because 97
 some weak back reflections of the CO₂-laser beams led 98
 to a slight undesirable corrugation of the optical poten- 99
 100 tial. This complicated the quantitative analysis of the 101
 BEC. Beams B₁ and B₂ are derived from a broadband 102
 fiber laser⁵ at 1064 nm. The powers in these beams are 103
 ramped up within 1.5 s to a maximum power of 70 mW 104
 for B₁ and 270 mW for B₂. The trapping in the dimple 105
 is now briefly done by all four laser beams with B₁ provid- 106
 ing most of the radial and A₁ most of the axial confine- 107
 ment. After switching off beam A₂ we measure the radial 108
 and axial trap frequencies in the dimple to (221.2 ± 1.6) 109
 Hz and (14.2 ± 0.1) Hz, respectively. During the ramp- 110
 ing up phase of B₁ and B₂ we reduce the magnetic field 111
 offset to 23 G and thus the scattering length to $300 a_0$ 112
 in order to reduce losses from three-body recombination 113
 [28]. The trap now contains about 1.7×10^6 atoms at a 114
 peak phase space density of approximately 0.13. 115

3.5 Forced evaporation towards BEC

116 We start forced evaporative cooling by ramping down 117
 118 the power in all three remaining beams. Simultaneously 119
 120 we remove the reservoir by switching off the CO₂-laser 121
 122 A₂ that is not responsible for axial confinement. To as- 123
 124 sure a well-defined ramp over a large intensity range we 125
 126 control the light power of the near-infrared beam B₁ by 127
 means of a logarithmic photodiode and a servo loop. The 128
 power in CO₂-laser beam A₁ is ramped to zero within 129
 5.5 s so that B₂ at the end of evaporation exclusively as- 130
 sures axial confinement. The change in beam pointing for 131
 A₂ does not affect the evaporation. For B₁ we approxi- 132

⁵ IPG Laser PVL-10

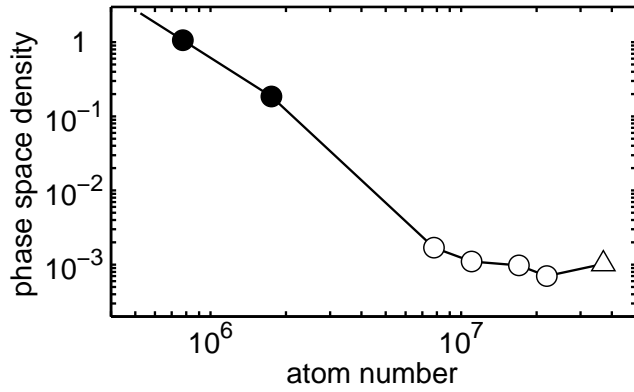


Fig. 3 Peak phase space density as function of atom number. The path of evaporation proceeds from right to left. The *triangle* shows the atomic ensemble immediately after lattice cooling. The *open circles* show the ensemble in the reservoir trap after 0.08, 0.22, 0.64, and 2.0 s. The *filled circles* correspond to the sample in dimple trap right after loading and after 1.5 s of evaporation. The phase transition occurs after 2 s of forced evaporation with $\sim 5 \times 10^5$ atoms left in the dimple trap.

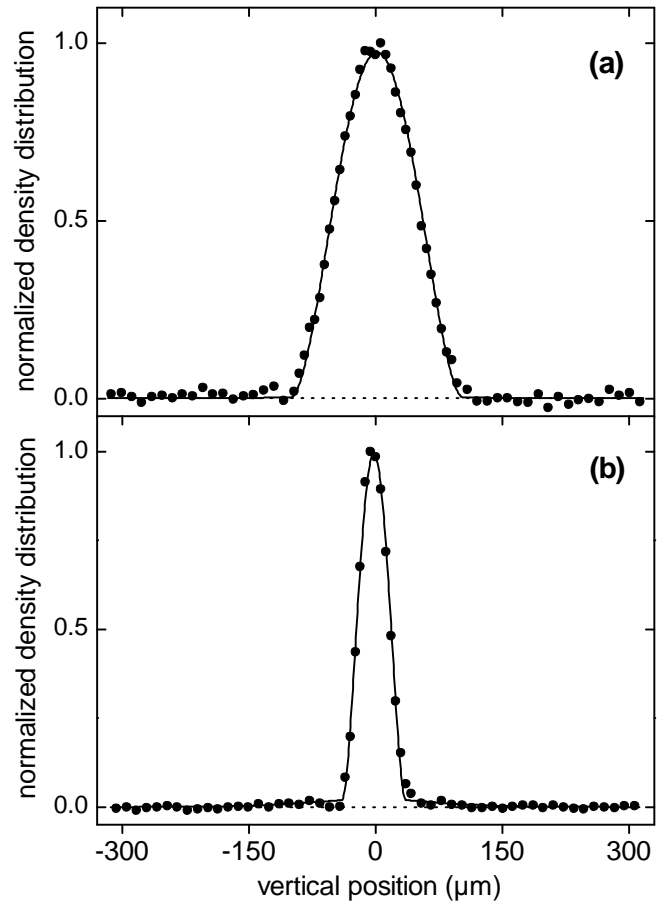


Fig. 4 Vertical density profiles of Cs condensates after 100 ms of free expansion in the levitation field. The solid curves are fits to the data for the Thomas-Fermi profiles which include possible thermal components. For better distinction the baseline is dashed. (a) Expansion with no change in scattering length. The total number of atoms in the condensate is $N = 1.1 \times 10^5$. (b) Expansion near zero scattering length under the same conditions reveals a small thermal component with a temperature of about 10 nK.

1 mately follow an exponential ramp over 5.5 s. The power
 2 in beam B_2 is only slightly reduced. The final power in
 3 B_1 and B_2 is 0.5 mW and 220 mW. We find and optimize
 4 this ramp by extending the ramp in discrete time steps
 5 of a few hundred milliseconds at the beginning and up
 6 to one second towards the end of the ramp.

7 At each step we search for a maximum in evaporation
 8 efficiency $\gamma = \log(D'/D)/\log(N/N')$ as a function of the
 9 trap depth and scattering length [34]. Here, D and D'
 10 are the phase-space densities at the beginning and end
 11 of each step, N and N' denote the respective particle
 12 numbers. Maximizing γ at each step results in an overall
 13 optimization of the evaporation path. We find that a
 14 magnetic field value of 21 G with scattering length $a =$
 15 $210 a_0$ is optimal during the forced evaporation phase.
 16 As can be seen from Fig. 3 the efficiency γ lies around
 17 3 during the forced evaporation ramp. We attribute this
 18 high efficiency to the fact that atoms can escape the trap
 19 into almost all directions because of the levitation field.
 20 We observe the phase transition after 2 s of forced evapo-
 21 rative cooling with about 5×10^5 atoms at a temperature
 22 of (200 ± 10) nK. At this point the power in beams B_1
 23 and B_2 is 8.7 mW and 250 mW. The duration of the
 24 ramp is relatively short. Our evaporation proceeds close
 25 to the hydrodynamic regime. Thus, significant improve-
 26 ment of the evaporation is not to be expected.

27 Further evaporation leaves a cigar-shaped condensate
 28 with the long axis in the horizontal plane. In Fig. 4 we
 29 show vertical density profiles of expanding condensates.
 30 The tunability of the scattering length allows us to ex-
 31 plore different regimes of expansion. For Fig. 4(a) we
 32 expand the condensate at the creation scattering length
 33 of $210 a_0$. This is the usual type of self-similar expansion
 34 in which the condensate in the Thomas-Fermi regime re-

tains its parabolic shape [35]. For Fig. 4(b) we step the
 scattering length to zero at the moment of release from
 the trap. The mean-field interaction thus vanishes and
 the rate of expansion is greatly reduced. This exposes a
 small thermal component, for which a bimodal fit reveals
 a temperature of around 10 nK. The critical tempera-
 ture at these trapping conditions is 24 nK, therefore the
 expected condensate fraction agrees well with the mea-
 sured value of 91%. From the fit to the data in Fig. 4
 we obtain that there are up to 1.1×10^5 atoms in the
 condensate with a 20% calibration error. The error does
 not come from the fit but from the overall uncertainty in
 determining the atom number. Usually, the error from
 absorption imaging alone is around 50%, but we can cali-
 brate the atom number from measurements on the chemi-
 cal potential, see Sec. 4.1. For this particular experiment
 we measure the final trap frequencies to (4.3 ± 0.2) Hz

and (21.1 ± 0.2) Hz along the axial and radial direction, respectively. We thus infer for the initial Thomas-Fermi sizes $R_r^{TF} = (8.7 \pm 0.3) \mu\text{m}$ and $R_a^{TF} = (42.5 \pm 1.2) \mu\text{m}$ along the radial and axial directions at a scattering length of $a = 210 a_0$. The peak density of the condensate is $n_0 = (2.1 \pm 0.1) \times 10^{13} \text{ cm}^{-3}$.

4 Tunable quantum gas

We now test the tunability of the condensate interaction. We first study the condensate expansion as a function of scattering length [36] in two different ways. We then specialize to the case when the interaction energy is switched off and present improved results on the ultra-slow expansion of the condensate in comparison with earlier measurements in [4]. Finally, we excite compression oscillations of the trapped condensate by suddenly stepping the scattering length to a lower value.

4.1 Expansion energy as a function of scattering length

We measure the release energy of the condensate for slow and fast changes of the scattering length. When we slowly vary the scattering length the wave function of the trapped condensate can follow adiabatically and the condensate remains in equilibrium. The release energy is proportional to the chemical potential of the condensate at the given value of the scattering length. The situation is different when we rapidly switch the scattering length at the moment of condensate release. The condensate then expands from a non-equilibrium state because the wave function has not had time to adjust to the change in interaction energy. This leads to strong changes for the rate of condensate expansion in comparison to the expansion from equilibrium.

We first consider a condensate in the Thomas-Fermi regime for which we adiabatically ramp the scattering length to a new value. For such a condensate, the release energy E_{rel} directly corresponds to the chemical potential μ_{TF} through $\frac{7}{2}E_{rel} = \mu_{TF}$ [35], which is given by

$$\mu_{TF} = \frac{\hbar \bar{\nu}}{2} \left(\frac{15 N}{a_{ho}} \right)^{2/5} a^{2/5}. \quad (1)$$

Here, $\bar{\nu}$ is the geometric average of the trap frequencies, N is the particle number in the condensate, and $a_{ho} = \sqrt{\hbar/(m 2\pi \bar{\nu})}$ is the oscillator length. For the experiment we produce a condensate with $N = 8.5 \times 10^4$ atoms at a creation scattering length of $a_c = 210 a_0$. We then slowly ramp the magnetic field to values between 20 and 35 G, setting the scattering length to a value between about 200 and 700 a_0 . The slow ramping excludes values below the Feshbach resonance at 19.9 and above the one at 48.0 G because of strong loss⁶. The condensate is then released from the trap and we measure the release energy. The results are shown in Fig. 5. Here we assume that the magnetic field strength translates into scattering length according to Fig. 1. The data is well fit by a function of the form $C a^{2/5}$ according to Eq. (1). From the fit parameter C we can deduce an independent

⁶ A combination of slow ramping and quick jumping at the Feshbach resonances would allow access to the full range of

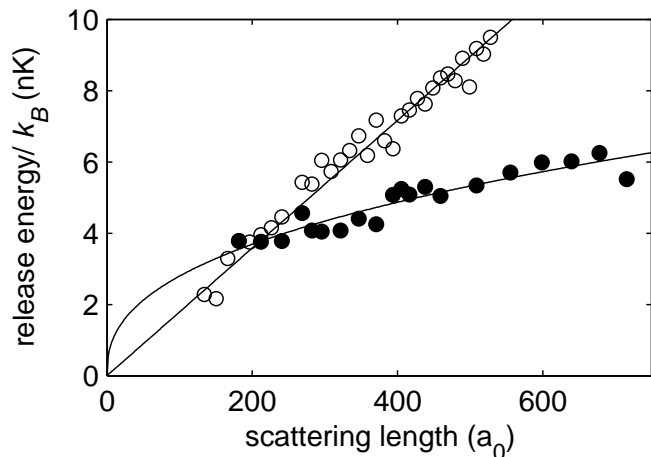


Fig. 5 Release energy of the condensate as a function of scattering length a . The *filled circles* represent experimental data for the case of adiabatic ramping of a trapped condensate. The data, corresponding to $2/7$ of the chemical potential at a given value of the scattering length, is fit by $C a^{2/5}$. The *open circles* represent data for rapid switching at the moment of condensate release. As discussed in the text, the straight line is not a fit. It connects the origin with the fitted value of the release energy at the creation scattering length.

estimate of the particle number $N = (8.2 \pm 1.3) \times 10^4$. The error is dominated by the error in determining the trap frequencies.

For a sudden change of the scattering length the condensate wave function has no time to react. For example, for an increase of the scattering length the density distribution is too narrow in comparison to the equilibrium density distribution at the new value of the scattering length. The condensate thus expands more rapidly than a condensate in equilibrium at this new value. Since the mean-field interaction energy of the condensate scales linearly with the scattering length for a given density profile [35], we expect a linear behavior of the release energy as a function of the final scattering length a . In Fig. 5 we thus compare the data for the measured release energy to a straight line $C a_c^{2/5} a/a_c$ given by the origin and the fitted value of the release energy at the creation scattering length $a_c = 210 a_0$. We find good agreement with the linear dependence.

4.2 Ultra-slow condensate expansion

We now study the expansion of the condensate near the zero-crossing of the scattering length. At the moment of condensate release, we rapidly switch the magnetic field from the creation field near 20 G to (17.17 ± 0.05) G, corresponding to $a = (3.4 \pm 3.0) a_0$. The error in determining the precise magnetic field at the position of condensate requires that we choose a slightly positive value of the scattering length to assure that no weakly attractive interactions modify the condensate expansion. The levitation field remains on, allowing for an extended observation period because the atoms then do not fall under

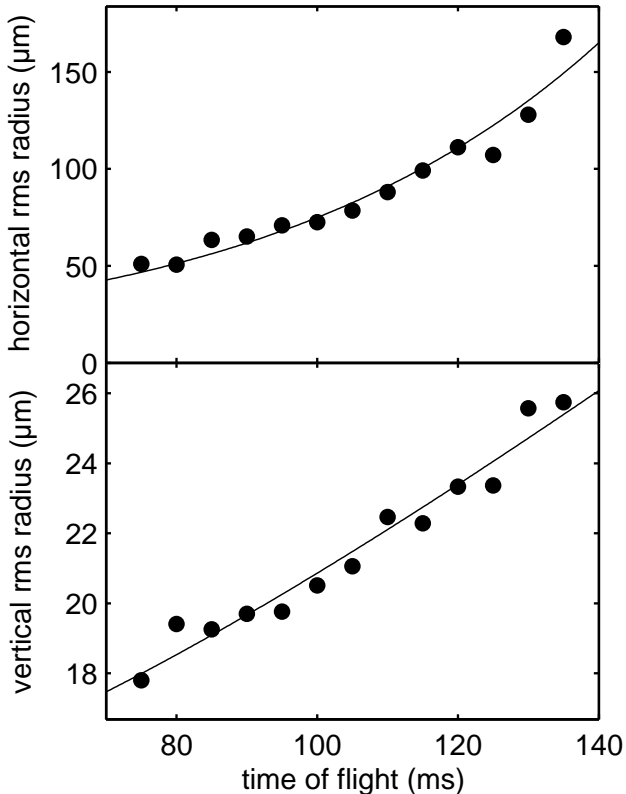


Fig. 6 Expansion of the non-interacting condensate. The data points show the horizontal (above) and vertical (below) rms radius of the BEC as a function of expansion time near the zero crossing of scattering length. Note the different scales. The fit to the residual vertical expansion reveals a release energy of $k_B \times (51 \pm 3)$ pK. For the horizontal expansion the data is fit by $A \cosh(\alpha t)$ with $\alpha = 2\pi \times (3.20 \pm 0.23)$ Hz.

gravity. Fig. 6 shows the vertical and horizontal extent of a BEC with 1.2×10^5 atoms as a function of time after release from the trap. We only show the data after 75 ms of expansion when the optical density of the atomic cloud is sufficiently reduced to allow for reliable absorption imaging. The horizontal expansion is dominated by the magnetic anti-trapping potential which derives from the presence of the levitation field and which magnifies the atomic cloud according to the cosine hyperbolicus function, see Sec. 3.3. The measured rate of expansion $2\pi \times (3.20 \pm 0.23)$ Hz agrees reasonably well with the expected rate constant $\alpha = 2\pi \times 3.4$ Hz. The vertical expansion corresponds to a release energy of $k_B \times (51 \pm 3)$ pK. Note that this is much lower than the kinetic energy of the ground state $\hbar\omega_r/4 = k_B \times 253$ pK given by a radial trap frequency of $\omega_r = 2\pi \times 21.1$ Hz. It is remarkable that the release energy is less than the zero-point energy of the ground state. Since the spatial extent of the condensate is much larger than the size of the ground state wave function of the harmonic oscillator, the momentum spread, limited by the uncertainty of the wave function

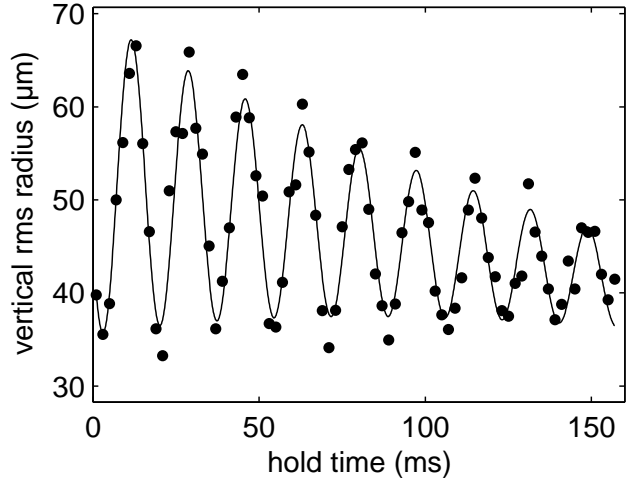


Fig. 7 Condensate oscillations after rapid switching of the scattering length. The filled circles show the vertical rms radius of an expanding BEC with 7×10^4 atoms after 80 ms of free expansion as a function of hold time in the trap. The scattering length has been switched rapidly from $363 a_0$ to $25 a_0$. The solid curve is a fit to the data giving an oscillation frequency of (58.3 ± 0.2) Hz. We independently measure the radial trap frequency to (28 ± 1) Hz.

of the initial condensate, is lower than that of the ground state.

4.3 Condensate oscillations

By rapidly ramping the scattering length it is possible to excite oscillations of the condensate in the trap [37]. In fact, in the limit of a cigar shaped condensate one expects radial “compression” or “expansion oscillations” at twice the trap frequency. Compression oscillations can be seen in Fig. 7 where we plot the vertical radius of the released condensate as a function of hold time t_h in the trap. To excite the oscillation we step the scattering length from a value of $a = 363 a_0$ ($B = 24.4$ G) to $a = 25 a_0$ ($B = 17.6$ G) at time t_0 . The condensate is then allowed to oscillate in the trap for a variable hold time t_h at the final value of the scattering length. We release the condensate at time $t_0 + t_h$ and take an image after 80 ms of free expansion. We fit the data by a sinusoidal function. The measured compression oscillation frequency of (58.3 ± 0.2) Hz agrees well with twice the radial trap frequency of $2 \times (28 \pm 1)$ Hz at the given trapping power. To account for the damping we have to introduce an exponential decay of the amplitude and of the offset value. The damping of the amplitude has a time constant of 126 ms. We have not yet identified the origin of this damping. Possibly the BEC samples different trapping frequencies due to the large amplitude of the oscillation, which would lead to an apparent damping. Also, damping might be caused by the interaction

with a residual thermal cloud or by parametric processes [38].

5 Conclusion

We have shown that essentially pure Cs condensates can be produced with more than 10^5 atoms. In our optical trap it is possible to flexibly change the atomic scattering properties. The atomic condensate can now be used as the starting point for experiments where a tuning and ramping of the scattering properties can be exploited. It will be interesting to study the case of a non-interacting condensate at the zero-crossing of the scattering length. Such a condensate might be used in atom interferometers where one wishes to suppress any mean-field effects [39]. On the other hand, tuning to large values of the scattering length might allow the investigation of effects beyond the mean-field approximation [35]. Also, modulation of the scattering length could be used as an alternative tool to probe the excitation spectrum of the condensate. Finally, ultracold Cs₂ molecules can be created by ramping across one of the Feshbach resonances [8] and the transition from an atomic to a molecular condensate could then be studied.

Acknowledgements This work is supported by the Austrian “Fonds zur Förderung der wissenschaftlichen Forschung” (FWF) within SFB 15 (project part 16) and by the European Union in the frame of the Cold Molecules TMR Network under Contract No. HPRN-CT-2002-00290. M.M. is supported by DOC [Doktorandenprogramm der Österreichischen Akademie der Wissenschaften]. C.C. is supported by a Lise-Meitner-Fellowship from the FWF.

References

1. M. Barrett, J. Sauer, M. Chapman: Phys. Rev. Lett. **87**, 010404 (2001)
2. Y. Takasu, K. Maki, K. Komori, T. Takano, K. Honda, M. Kumakura, T. Yabuzaki, Y. Takahashi: Phys. Rev. Lett. **91**, 040404 (2003)
3. G. Cennini, G. Ritt, C. Geckeler, M. Weitz: Phys. Rev. Lett. **91**, 240408 (2003)
4. T. Weber, J. Herbig, M. Mark, H.-C. Nägerl, R. Grimm: Science **299**, 232 (2003)
5. D. Rychtarik, B. Engeser, H.-C. Nägerl, R. Grimm: Phys. Rev. Lett. **92**, 173003 (2004)
6. C. Chin, A. J. Kerman, V. Vuletic, S. Chu: Phys. Rev. Lett. **90**, 033201 (2003)
7. C. A. Regal, C. Ticknor, J. L. Bohn, D. S. Jin: Nature **424**, 47 (2003)
8. J. Herbig, T. Kraemer, M. Mark, T. Weber, C. Chin, H.-C. Nägerl, R. Grimm: Science **301**, 1510 (2003)
9. S. Dürr, T. Volz, A. Marte, G. Rempe: Phys. Rev. Lett. **92**, 020406 (2004)
10. K. Xu, T. Mukaiyama, J. R. Abo-Shaeer, J. K. Chin, D. E. Miller, W. Ketterle: Phys. Rev. Lett. **91**, 210402 (2003)
11. S. Jochim, M. Bartenstein, A. Altmeyer, G. Hendl, S. Riedl, C. Chin, J. Hecker Denschlag, R. Grimm: Science **302**, 2101 (2003)
12. M. Greiner, C. A. Regal, D. S. Jin: Nature **426**, 537 (2003)
13. C. Chin, V. Vuletic, A. J. Kerman, S. Chu, E. Tiesinga, P. J. Leo, C. J. Williams: Phys. Rev. A to appear
14. E. A. Donley, N. R. Claussen, S. T. Thomson, C. E. Wieman: Nature **417**, 529 (2002)
15. L. Radzihovsky, J. Park, P. B. Weichman: Phys. Rev. Lett. **92**, 160402 (2004)
16. M. W. J. Romans, R. A. Duine, S. Sachdev, H. T. C. Stoof: Phys. Rev. Lett. **93**, 020405 (2004)
17. J. Söding, D. Guéry-Odelin, P. Desbiolles, G. Ferrari, J. Dalibard: Phys. Rev. Lett. **80**, 1869 (1998)
18. J. Arlt, P. Bance, S. Hopkins, J. Martin, S. Webster, A. Wilson, K. Zetie, C. J. Foot: J. Phys. B **31**, L321 (1998)
19. D. Guéry-Odelin, J. Söding, P. Desbiolles, J. Dalibard: Europhys. Lett. **44**, 26 (1998)
20. D. Guéry-Odelin, J. Söding, P. Desbiolles, J. Dalibard: Optics Express **2**, 323 (1998)
21. S. A. Hopkins, S. Webster, J. Arlt, P. Bance, S. Cornish, O. Maragò, C. J. Foot: Phys. Rev. A. **61**, 032707 (2000)
22. P. J. Leo, E. Tiesinga, P. S. Julienne, D. K. Walter, S. Kadlecek, T. G. Walker: Phys. Rev. Lett. **81**, 1389 (1998)
23. A. M. Thomas, S. Hopkins, S. L. Cornish, C. J. Foot: J. Opt. B **5**, S107 (2003)
24. H. Perrin, A. Kuhn, I. Bouchoule, C. Salomon: Europhys. Lett. **42**, 395 (1998)
25. V. Vuletić, A. J. Kerman, C. Chin, S. Chu: Phys. Rev. Lett. **82**, 1406 (1999)
26. M. Hammes, D. Rychtarik, V. Druzhinina, U. Moslener, I. Manek-Hönninger, R. Grimm: J. Mod. Opt. **47**, 2755 (2000)
27. D.-J. Han, M. T. DePue, D. S. Weiss: Phys. Rev. A **63**, 023405 (2001)
28. T. Weber, J. Herbig, M. Mark, H.-C. Nägerl, R. Grimm: Phys. Rev. Lett. **91**, 123201 (2003)
29. D. J. Han, Marshall T. DePue, David S. Weiss: Phys. Rev. A **63**, 023405 (2001)
30. A. J. Kerman, V. Vuletić, C. Chin, S. Chu: Phys. Rev. Lett. **84**, 439 (2000)
31. D. M. Stamper-Kurn, H.-J. Miesner, A. P. Chikkatur, S. Inouye, J. Stenger, W. Ketterle: Phys. Rev. Lett. **81**, 2194 (1998)
32. T. Weber: PhD thesis, Univ. Innsbruck 2003
33. P. Treutlein, K. Y. Chung, S. Chu: Phys. Rev. A **63**, 051401 (2001)
34. W. Ketterle, N. J. Van Druten: Adv. At. Mol. Opt. Phys. **37**, 181 (1996)
35. L. Pitaevskii, S. Stringari: *Bose-Einstein Condensation* (Clarendon Press, Oxford 2003)
36. S. L. Cornish, N. R. Claussen, J. L. Roberts, E. A. Cornell, C. E. Wieman: Phys. Rev. Lett. **85**, 1795 (2000)
37. Y. Kagan, E. L. Surkov, G. V. Shlyapnikov: Phys. Rev. Lett. **79**, 2604 (2001)
38. F. Chevy, V. Bretin, P. Rosenbusch, K. W. Madison, J. Dalibard: Phys. Rev. Lett. **88**, 250402 (2002)
39. S. Gupta, K. Dieckmann, Z. Hadzibabic, D. E. Pritchard: Phys. Rev. Lett. **89**, 140401 (2002)